INTERNATIONAL JOURNAL FOR NUMERICAL AND ANALYTICAL METHODS IN GEOMECHANICS
Int. J. Numer. Anal. Meth. Geomech. 2013; **37**:3278–3292
Published online 29 April 2013 in Wiley Online Library (wileyonlinelibrary.com). DOI: 10.1002/nag.2193

Assessment of slope stability in cohesive soils due to a rainfall

S. Pietruszczak*,† and E. Haghighat

Department of Civil Engineering, McMaster University, Hamilton, Ontario, Canada

SUMMARY

The primary focus in this work is on proposing a methodology for the assessment of stability of natural/engineered slopes in clayey soils subjected to water infiltration. In natural deposits of fine-grained soils, the presence of water in the vicinity of minerals results in an interparticle bonding. This effect cannot be easily quantified as it involves complex chemical interactions at the micromechanical level. Here, the evolution of strength properties, including the apparent cohesion resulting from initial suction at the irreducible fluid saturation, is described by employing the framework of chemoplasticity. The paper provides first the formulation of the problem; this involves specification of the constitutive relation, development of an implicit return mapping scheme, and the outline of a coupled transient formulation. The framework is then applied to examine the stability of a slope subjected to a prolonged period of intensive rainfall. It is shown that the water infiltration may trigger the loss of stability resulting from the degradation of material properties. Copyright © 2013 John Wiley & Sons, Ltd.

Received 1 August 2012; Revised 20 December 2012; Accepted 12 March 2013

KEY WORDS: chemoplasticity; rainfall infiltration; slope stability; unsaturated flow

1. INTRODUCTION

It is well known that a period of heavy rainfall can trigger a loss of stability of slopes. This is particularly the case for slopes constructed in cohesive soils, such as clay or a cemented soil, where the water infiltration leads to a chemical interaction resulting in degradation of mechanical properties of the material.

The problem of stability of natural and engineered slopes has been a subject of research for a number of decades. In particular, the notion of influence of suction pressure on the stability has become an important issue. In recent years, several case histories have been documented (e.g., in Hong Kong, Korea, Malaysia, and Singapore) whereby the loss of stability was related to the loss of suction triggered by the local weather conditions [1–3].

The primary difficulty in modeling the loss of stability due to a heavy rainfall lies in assessing the *in situ* conditions and in describing the coupling between the time-dependent process of water infiltration and the evolution of stress field. The problem is typically analyzed by integrated software in which the transient seepage analysis is coupled with traditional limit equilibrium slope stability analysis [4–6]. Alternatively, the frameworks for unsaturated soil are implemented in which the suction pressure is considered as a state parameter and an optimization technique is used to search for a critical slip surface (e.g., [4]). In general, the conventional methods for assessing the stability of unsaturated soils, based on limit equilibrium approach, significantly underestimate the safety factors. Therefore, more accurate techniques are required.

Specification of properties of clays is difficult as it involves a very complex system of mineralogical and chemical factors. There are significant variations in the composition, size, and relative orientation

*Correspondence to: S. Pietruszczak, Civil Engineering Department, McMaster University, Hamilton, Ontario, Canada.
†E-mail: pietrusz@mcmaster.ca

of the mineral phase, as well as the composition and amount of the aqueous phase. Therefore, a micromechanically based description of physical properties of clays represents an overwhelming task.

In clays, the bond strength increases rapidly with decreasing water content. It is rather apparent that free water in clays has low compressibility and virtually no viscosity. The water in the vicinity of minerals, however, has quite different properties that cannot, in fact, be quantified because of complex chemical interactions. Therefore, the measurement and/or control of suction pressures are difficult. Recognizing the aforementioned limitations, a different methodology is proposed here which is an alternative to a micromechanical approach. At the range of irreducible saturation (cf. [7]), when the water phase is discontinuous, the behavior of the material is described based on a phenomenological framework of chemoplasticity (cf. [8–10]). Within this framework, an increase in water content due to wetting is said to trigger a reduction in the interparticle bonding and the corresponding degradation of strength and deformation properties at the macroscale. At the stage when the water phase becomes continuous, the behavior can then be defined in mechanical terms alone, for example, by employing an averaging procedure in which the compressibility of the mixture is expressed as a function of properties of constituents (free water and air) and the microstructure of saturation ([11, 12]). Note that such an approach incorporates the average 'pore size' as an independent characteristic dimension. Alternatively, the problem may be phrased using the classical notions of unsaturated soil mechanics [13–15].

In the next section, the formulation of the problem is discussed including the development of implicit (backward Euler) integration scheme. Later, the governing equations describing the transient hydromechanical coupling are reviewed, and the framework is applied to examine the stability of a slope in cohesive soil, subjected to a period of intense rainfall. In solving the problem, the evolution of the phreatic surface is monitored and is coupled with mechanical analysis incorporating the chemical interaction.

2. FORMULATION OF THE PROBLEM

2.1. Constitutive relation

The general approach for describing the evolution of properties of clays in the presence of the interparticle bonding is based on the framework of chemoplasticity, similar to that of Ref. [10]. Within this approach, the progress in chemomechanical interaction is monitored by a scalar parameter ζ. Here, this parameter may be interpreted as the change in the initial suction pressure u_s^0, at the irreducible wetting fluid saturation, in Representative Elementary Volume (REV); i.e. $\zeta \propto \left(u_s^0 - u_s\right)/u_s^0$, so that $\zeta \subset [0,1]$.

The evolution law can be taken in a simple linear form

$$\frac{\partial \zeta}{\partial t'} = B(1-\zeta); \quad \mathrm{d}t' = \mathrm{g}\mathrm{d}t \tag{1}$$

where $\mathrm{g} \subset [0,1]$ depends on the chemical composition of the clay minerals and water, and B is a material constant. In the elastic range, the constitutive relation takes the form

$$\boldsymbol{\varepsilon}^e = \mathbb{D}^{-1} : \boldsymbol{\sigma} \quad \rightarrow \quad \dot{\boldsymbol{\varepsilon}}^e = \mathbb{D}^{-1} : \dot{\boldsymbol{\sigma}} + \dot{\mathbb{D}}^{-1} : \boldsymbol{\sigma} = \mathbb{D}^{-1} : \dot{\boldsymbol{\sigma}} + \dot{\zeta}\, \partial_\zeta \mathbb{D}^{-1} : \boldsymbol{\sigma} \tag{2}$$

where $\boldsymbol{\sigma}$ is the *effective* stress and $\mathbb{D}^{-1}$ is the elastic compliance operator. Note that the differential form of Eq. (2) may be expressed as

$$\dot{\boldsymbol{\sigma}} = \mathbb{D} : \dot{\boldsymbol{\varepsilon}}^e - \dot{\zeta}\left(\mathbb{D} : \partial_\zeta \mathbb{D}^{-1}\right) : \boldsymbol{\sigma} \tag{3}$$

Invoking now the additivity postulate, total strain rate can be written as

$$\dot{\boldsymbol{\varepsilon}} = \dot{\boldsymbol{\varepsilon}}^e + \dot{\boldsymbol{\varepsilon}}^p + \dot{\boldsymbol{\epsilon}} \tag{4}$$

where $\dot{\boldsymbol{\epsilon}}$ is the volumetric strain rate due to wetting. The latter may be taken as $\dot{\boldsymbol{\epsilon}} = \epsilon\dot{\zeta}\mathbf{I}$, where ϵ is the maximum expansion/contraction in the stress-free state. The plastic strain rates $\dot{\boldsymbol{\varepsilon}}^p$ are defined following standard plasticity formalism, that is,

DOI: 10.1002/nag

$$f = f(\boldsymbol{\sigma}, \kappa, \zeta) \leq 0; \quad \dot{\boldsymbol{\varepsilon}}^p = \dot{\lambda} \frac{\partial \psi}{\partial \boldsymbol{\sigma}} \tag{5}$$

where $f=f(\boldsymbol{\sigma},\kappa,\zeta)$ is the yield function, $\kappa = \kappa(\dot{\boldsymbol{\varepsilon}}^p)$ is the hardening parameter, and $\psi = \psi(\boldsymbol{\sigma},\zeta)$ is the plastic potential function.

By using the decomposition (4), the constitutive relation defining the stress rate may be expressed as

$$\dot{\boldsymbol{\sigma}} = \mathbb{D} : (\dot{\boldsymbol{\varepsilon}} - \dot{\boldsymbol{\epsilon}}) - \mathbb{D} : \dot{\boldsymbol{\varepsilon}}^p - \dot{\zeta} \left(\mathbb{D} : \partial_\zeta \mathbb{D}^{-1} \right) : \boldsymbol{\sigma} \tag{6}$$

2.2. Implicit integration scheme

The constitutive relation defined by Eq. (6) is subjected to the following constraints

$$\begin{matrix} f = f(\boldsymbol{\sigma}, \kappa, \zeta) \leq 0 \\ \dot{\lambda} \geq 0 \end{matrix} \quad \rightarrow \quad f\dot{\lambda} = 0 \tag{7}$$

During an active loading process, there is $\dot{\lambda} > 0$ and $f(\boldsymbol{\sigma},\kappa,\zeta)=0$, so that $\dot{f}(\boldsymbol{\sigma}, \kappa, \zeta) = 0$. The latter represents the consistency condition and takes the form

$$\dot{f} = \frac{\partial f}{\partial \boldsymbol{\sigma}} : \dot{\boldsymbol{\sigma}} + \frac{\partial f}{\partial \kappa} \dot{\kappa} + \frac{\partial f}{\partial \zeta} \dot{\zeta} = 0 \tag{8}$$

Following now the general return mapping scheme [16, 17], the stress and plastic strain at time $t+\Delta t$ can be expressed as

$$\begin{aligned} \boldsymbol{\varepsilon}^p_{t+\Delta t} &= \boldsymbol{\varepsilon}^p_t + \dot{\boldsymbol{\varepsilon}}^p_{t+\Delta t} \Delta t \\ &= \boldsymbol{\varepsilon}^p_t + \Delta\lambda_{t+\Delta t} \partial_{\boldsymbol{\sigma}} \psi(\boldsymbol{\sigma}_{t+\Delta t}, \zeta_{t+\Delta t}) \\ \boldsymbol{\sigma}_{t+\Delta t} &= \boldsymbol{\sigma}_t + \dot{\boldsymbol{\sigma}}_{t+\Delta t} \Delta t \\ &= \mathbb{D}_{t+\Delta t} : (\Delta\boldsymbol{\varepsilon} - \Delta\boldsymbol{\epsilon})_{t+\Delta t} - \mathbb{D}_{t+\Delta t} : \Delta\boldsymbol{\varepsilon}^p_{t+\Delta t} - \Delta\zeta_{t+\Delta t} \left(\mathbb{D} : \partial_\zeta \mathbb{D}^{-1} \right)_{t+\Delta t} : \boldsymbol{\sigma}_{t+\Delta t} \end{aligned} \tag{9}$$

Dropping the subscript $t+\Delta t$ and solving the second equation for $\boldsymbol{\sigma}_{t+\Delta t}$, one obtains

$$\begin{aligned} \boldsymbol{\varepsilon}^p &= \boldsymbol{\varepsilon}^p_t + \Delta\lambda \, \partial_{\boldsymbol{\sigma}} \psi \\ \boldsymbol{\sigma} &= \mathbb{A}^{-1} : (\boldsymbol{\sigma}_t + \mathbb{D} : (\Delta\boldsymbol{\varepsilon} - \Delta\boldsymbol{\epsilon}) - \mathbb{D} : \Delta\boldsymbol{\varepsilon}^p) \end{aligned} \tag{10}$$

where $\mathbb{A} = \mathbb{I} + \Delta\zeta \left(\mathbb{D} : \partial_\zeta \mathbb{D}^{-1} \right)$. Note that the primary unknowns here are $\boldsymbol{\sigma} = \boldsymbol{\sigma}_{t+\Delta t}$ and $\Delta\lambda = \Delta\lambda_{t+\Delta t}$, whereas the parameter κ is a scalar valued function of plastic deformation, so that it is a dependent variable.

To solve the aforementioned set of equations, the general Newton–Raphson procedure is implemented. Following this scheme, the residuals can be defined as

$$\begin{aligned} \mathbf{r}_k &= \boldsymbol{\sigma}_k - \mathbb{A}^{-1} : \left(\boldsymbol{\sigma}_t + \mathbb{D} : (\Delta\boldsymbol{\varepsilon} - \Delta\boldsymbol{\epsilon}) - \mathbb{D} : \Delta\boldsymbol{\varepsilon}^p_k \right) \\ &= \boldsymbol{\sigma}_k - \mathbb{A}^{-1} : (\boldsymbol{\sigma}_t + \mathbb{D} : (\Delta\boldsymbol{\varepsilon} - \Delta\boldsymbol{\epsilon}) - \Delta\lambda_k \, \mathbb{D} : \partial_{\boldsymbol{\sigma}} \psi_k) \\ f_k &= f(\boldsymbol{\sigma}_k, \kappa_k, \Delta\lambda_k) \end{aligned} \tag{11}$$

DOI: 10.1002/nag

Expanding these residuals, using Taylor expansion, yields

$$\begin{aligned} \mathbf{r}_k + \partial_{\boldsymbol{\sigma}} \mathbf{r}_k : \delta\boldsymbol{\sigma}_k + \partial_{\Delta\lambda} \mathbf{r}_k \delta\lambda_k = 0 \\ f_k + \partial_{\boldsymbol{\sigma}} f_k : \delta\boldsymbol{\sigma}_k + \partial_{\Delta\lambda} f_k \delta\lambda_k = 0 \end{aligned} \tag{12}$$

where $\partial_{\boldsymbol{\sigma}} \mathbf{r}_k = \mathbb{Q}_k = \left(\mathbb{I} + \Delta\lambda \left(\mathbb{A}^{-1} : \mathbb{D}\right) : \partial_{\boldsymbol{\sigma}\boldsymbol{\sigma}} \psi\right)_k$ and $\partial_{\Delta\lambda} \mathbf{r}_k = \left(\left(\mathbb{A}^{-1} : \mathbb{D}\right) : \partial_{\boldsymbol{\sigma}} \psi\right)_k$.

Solving now the aforementioned set of equation, one has

$$\delta\boldsymbol{\sigma}_k = -\mathbb{Q}_k^{-1} : \left(\mathbf{r}_k + \partial_{\Delta\lambda} \mathbf{r}_k \delta\lambda_k\right) \tag{13}$$

and

$$\delta\lambda_k = \frac{f_k - \partial_{\boldsymbol{\sigma}} f_k : \mathbb{Q}^{-1} : \mathbf{r}_k}{\partial_{\boldsymbol{\sigma}} f_k : \mathbb{Q}^{-1} : \mathbb{C} : \partial_{\boldsymbol{\sigma}} \psi_k - \partial_{\Delta\lambda} f_k} \tag{14}$$

which fully defines the stress and plastic strain corrections during the Newton–Raphson iterations.

To specify the tangential stiffness operator, which is required for the global Newton–Raphson solution algorithm, the stress increment can be expressed as

$$\Delta\boldsymbol{\sigma} = \mathbb{Q}^{-1} : \mathbb{A}^{-1} : \mathbb{D} : \left(\Delta\boldsymbol{\varepsilon} - \Delta\boldsymbol{\epsilon}\right) - \mathbb{Q}^{-1} : \mathbb{A}^{-1} : \mathbb{D} : \partial_{\boldsymbol{\sigma}} \psi \, \Delta\lambda \tag{15}$$

Defining now an operator $\mathbb{R} = \mathbb{Q}^{-1} : \mathbb{A}^{-1} : \mathbb{D}$ and using the consistency condition, one obtains

$$\begin{aligned} \Delta f &= \partial_{\boldsymbol{\sigma}} f : \Delta\boldsymbol{\sigma} + \partial_{\Delta\lambda} f : \Delta\lambda \\ &= \partial_{\boldsymbol{\sigma}} f : \mathbb{R} : \left(\Delta\boldsymbol{\varepsilon} - \Delta\boldsymbol{\epsilon}\right) - \left\{\partial_{\boldsymbol{\sigma}} f : \mathbb{R} : \partial_{\boldsymbol{\sigma}} \psi - \partial_{\Delta\lambda} f\right\} \Delta\lambda = 0 \end{aligned} \tag{16}$$

so that

$$\Delta\lambda = \frac{\partial_{\boldsymbol{\sigma}} f : \mathbb{R} : \left(\Delta\boldsymbol{\varepsilon} - \Delta\boldsymbol{\epsilon}\right)}{\partial_{\boldsymbol{\sigma}} f : \mathbb{R} : \partial_{\boldsymbol{\sigma}} \psi - \partial_{\Delta\lambda} f} \tag{17}$$

Thus, the stress increment may be written as

$$\Delta\boldsymbol{\sigma} = \mathbb{D}_T : \left(\Delta\boldsymbol{\varepsilon} - \Delta\boldsymbol{\epsilon}\right) \tag{18}$$

where $\mathbb{D}_T$, that is, the tangential stiffness operator, is defined as

$$\mathbb{D}_T = \mathbb{R} - \frac{\left(\mathbb{R} : \partial_{\boldsymbol{\sigma}} \psi\right) \otimes \left(\partial_{\boldsymbol{\sigma}} f : \mathbb{R}\right)}{\partial_{\boldsymbol{\sigma}} f : \mathbb{R} : \partial_{\boldsymbol{\sigma}} \psi - \partial_{\Delta\lambda} f} \tag{19}$$

In the numerical examples provided later, the aforementioned backward Euler scheme is combined with subincrementation. This is primarily because the chemical degradation is very fast, and small time increments are required to obtain an accurate solution for the local stress trajectories.

DOI: 10.1002/nag

3. APPLICATION OF CHEMOPLASTICITY FRAMEWORK TO MODELING OF SOIL INFILTRATION

3.1. Description of unsaturated flow in porous media

In order to trace the evolution of phreatic surface during the rainfall infiltration, the problem is defined by invoking a coupled formulation for flow through unsaturated porous media [18]. Within this framework, the porous material is considered as a mixture of solid grains and voids, the latter filled with water and/or air.

Neglecting the inertia forces, the momentum balance equation for the solid–fluid mixture takes the form

$$\nabla\cdot\hat{\boldsymbol{\sigma}} + \hat{\rho}\mathbf{g} = 0 \tag{20}$$

subject to

$$\begin{array}{ll} \mathbf{v} = \widetilde{\mathbf{v}} & \text{on} \quad \Gamma_d \\ \hat{\boldsymbol{\sigma}}\cdot\mathbf{n} = \widetilde{\mathbf{t}} & \text{on} \quad \Gamma_t \end{array} \tag{21}$$

Here, $\hat{\boldsymbol{\sigma}}$ is the *total* stress, $\mathbf{g}$ is the acceleration due to gravity, and $\widetilde{\mathbf{v}}$ and $\widetilde{\mathbf{t}}$ represent the velocity and traction prescribed on the boundaries Γ_d and Γ_t, respectively. Furthermore, $\hat{\rho}$ is the density of the mixture; the latter, neglecting the density of air, may be defined as $\hat{\rho} = (M_s + M_w)/V = (1-n)\rho_s + Sn\rho_w$, where n and S are the porosity and the degree of saturation, and the indexes s and w refer to solids and water, respectively.

For unsaturated soil, the stress transmitted by the skeleton, i.e. the effective stress $\boldsymbol{\sigma}$, is typically defined using Bishop's relation

$$\boldsymbol{\sigma} = \hat{\boldsymbol{\sigma}} - (\chi u_w + (1-\chi)u_a)\mathbf{I} \approx \hat{\boldsymbol{\sigma}} - \chi u_w \mathbf{I} \tag{22}$$

where $\mathbf{I}$ is the identity tensor, u_w and u_a are the water and air pressures, respectively, and χ is the Bishop's parameter. Apparently, if the air phase is continuous, the excess of air pressure is usually neglected, so that $u_a \to 0$ in Eq. (22).

Note again that at the range of irreducible saturation, when the aqueous phase is present only in the vicinity of minerals, the material is conceptually considered as a continuum with an apparent cohesion. At this stage, an increase in water content due to wetting activates the chemomechanical interaction and leads to a microstructure of saturation in which the water phase becomes continuous. For the latter scenario, the simulations presented here were completed by identifying the parameter χ with the degree of saturation S, which is consistent with a similar assumption adopted by other investigators (e.g., [19, 20]). It is noted, however, that the decomposition (22) is semi-empirical in nature and the problem may, in fact, be phrased by assuming $\chi \to 1$ (i.e., Terzaghi's principle) and considering specific features of the geometry of microstructure of saturation. As shown in Refs [11, 12], when the water phase is continuous, the evolution of suction pressure as well as the compressibility of the immiscible air–water mixture may be defined as an explicit function of the surface area of grains (or the air–water menisci) and the properties of constituents (i.e., free water/air).

Consider now the mass balance equation for the fluid phase, which may be expressed, after normalizing with respect to ρ_w^0, in the following form [18]

$$\frac{1}{\rho_w^0}\left(\frac{\mathrm{d}}{\mathrm{d}t}(\rho_w Sn) + \rho_w Sn\,\mathbf{I}:\dot{\boldsymbol{\varepsilon}} + \nabla\cdot(\rho_w Sn\mathbf{v}_w)\right) = 0 \tag{23}$$

Assuming that solid grains are undeformable while the water is linearly compressible, the following relations may be established for a representative differential volume $\mathrm{d}V = \mathrm{d}V_s + \mathrm{d}V_v = \mathrm{d}V_s + \mathrm{d}V_w + \mathrm{d}V_a$

DOI: 10.1002/nag

$$\frac{\rho_s}{\rho_s^0}=\frac{\mathrm{d}V_s^0}{\mathrm{d}V_s}=\frac{\mathrm{d}V_s-\Delta\mathrm{d}V_s}{\mathrm{d}V_s}\approx 1$$

$$\frac{\rho_w}{\rho_w^0}=\frac{\mathrm{d}V_w^0}{\mathrm{d}V_w}=\frac{\mathrm{d}V_w-\Delta\mathrm{d}V_w}{\mathrm{d}V_w}\approx 1+\frac{u_w}{K_w} \tag{24}$$

$$n=1-\frac{\mathrm{d}V_s}{\mathrm{d}V}=1-\frac{\mathrm{d}V_s}{\mathrm{d}V_s^0}\frac{\mathrm{d}V_s^0}{\mathrm{d}V^0}\frac{\mathrm{d}V^0}{\mathrm{d}V}=1-J_sJ^{-1}\left(1-n^0\right)$$

where $J=\mathrm{d}V/\mathrm{d}V^0=\det\mathbf{F}$ and $\mathbf{F}$ is the deformation gradient.

Substituting the aforementioned relations into Eq. (23) and taking time derivatives (note that $\dot{J}=J\mathbf{I}:\dot{\boldsymbol{\varepsilon}}$), the following expression is obtained

$$\frac{\rho_w}{\rho_w^0}S\left\{n+\frac{1-n^0}{J}\right\}\mathbf{I}:\dot{\boldsymbol{\varepsilon}}+\left\{\frac{Sn}{K_w}+\frac{\rho_w}{\rho_w^0}\frac{\mathrm{d}S}{\mathrm{d}u_w}n\right\}\dot{u}_w+\boldsymbol{\nabla}\cdot\left(\frac{\rho_w}{\rho_w^0}Sn\mathbf{v}_w\right)=0 \tag{25}$$

Introducing now the definitions

$$\alpha=\frac{\rho_w}{\rho_w^0}\left\{n+\frac{1-n^0}{J}\right\}$$

$$\frac{1}{Q}=\frac{Sn}{K_w}+\frac{\rho_w}{\rho_w^0}\frac{\mathrm{d}S}{\mathrm{d}u_w}n \tag{26}$$

the mass balance relation can be expressed as

$$S\alpha\mathbf{I}:\dot{\boldsymbol{\varepsilon}}+\frac{1}{Q}\dot{u}_w-\boldsymbol{\nabla}\cdot\left(\frac{\rho_w}{\rho_w^0}Sn\mathbf{v}_w\right)=0 \tag{27}$$

and is subjected to the following boundary conditions

$$\begin{aligned} u_w&=\widetilde{u}_w \quad \text{on} \quad \Gamma_w\\ Sn\mathbf{v}_w\cdot\mathbf{n}&=\widetilde{q} \quad \text{on} \quad \Gamma_q \end{aligned} \tag{28}$$

The fluid flow in porous media is governed by Darcy's law, which takes the form

$$Sn\mathbf{v}_w=-\hat{\mathbf{k}}\cdot\boldsymbol{\nabla}\phi \tag{29}$$

In the equation above, $\mathbf{v}_w$ is the relative velocity of water, ϕ is the piezometric head, and $\hat{\mathbf{k}}=k_s\mathbf{k}$ is the permeability of the skeleton, with $\mathbf{k}$ representing the permeability under fully saturated condition and $k_s=k_s(S)$. Note that if the soil is isotropic with respect to permeability, then $\hat{\mathbf{k}}=k_sk\mathbf{I}=\hat{k}\,\mathbf{I}$. The piezometric head can be expressed as $\phi=\mathbf{x}\cdot\mathbf{g}/g+u_w/g\rho_w$, where the first term defines the elevation head and g is the magnitude of the gravitational acceleration. Given the aforementioned definitions, Darcy's law may be written in an alternative form, as

$$Sn\mathbf{v}_w=-\frac{\hat{k}}{\rho_wg}\left(\boldsymbol{\nabla}u_w-\rho_w\mathbf{g}\right) \tag{30}$$

DOI: 10.1002/nag

Now, by using stress decomposition (22), the weak form of Eq. (20) can be expressed as

$$\int_\Omega \delta\dot{\boldsymbol{\varepsilon}} : \boldsymbol{\sigma}\, \mathrm{d}V - \int_\Omega \delta\dot{\boldsymbol{\varepsilon}} : \chi u_w \mathbf{I}\, \mathrm{d}V = \int_{\Gamma_t} \delta\mathbf{v}\cdot\widetilde{\mathbf{t}}\, \mathrm{d}S + \int_\Omega \delta\mathbf{v}\cdot\hat{\rho}\mathbf{g}\, \mathrm{d}V \tag{31}$$

where $\dot{\boldsymbol{\varepsilon}} = \boldsymbol{\nabla}^s\mathbf{v}$. Also, by using Darcy's law (30), the mass balance may be expressed in a weak form as

$$\begin{aligned} &\int_\Omega \delta u_w\, S\alpha\mathbf{I} : \dot{\boldsymbol{\varepsilon}}\, \mathrm{d}V + \int_\Omega \delta u_w\, \frac{1}{Q}\dot{u}_w\, \mathrm{d}V - \int_\Omega \boldsymbol{\nabla}\delta u_w \cdot \frac{\hat{k}}{\rho_w^0 g}\boldsymbol{\nabla} u_w\, \mathrm{d}V \\ &\quad = \int_{\Gamma_q} \delta u_w \frac{\rho_w}{\rho_w^0}\widetilde{q}\, \mathrm{d}V - \int_\Omega \boldsymbol{\nabla}\delta u_w \cdot \frac{\hat{k}}{\rho_w^0 g}\rho_w \mathbf{g}\, \mathrm{d}V \end{aligned} \tag{32}$$

Here, the velocity $\mathbf{v}$ and pressure u_w are both smooth and continuous functions that satisfy the boundary conditions, that is,

$$\begin{aligned} &\mathbf{v} \in U, \quad U = \left\{ \mathbf{v} \mid \mathbf{v} \in \mathcal{C}^0 \ , \quad \mathbf{v} = \widetilde{\mathbf{v}} \quad \text{on} \quad \Gamma_d \right\} \\ &u_w \in V, \quad V = \left\{ u_w | u_w \in \mathcal{C}^0 \ , \quad u_w = \widetilde{u}_w \quad \text{on} \quad \Gamma_w \right\} \end{aligned} \tag{33}$$

where U and V are the set of kinematically admissible velocity and pressure spaces. Note that $\delta\mathbf{u}$ and δu_w are also required to have similar properties as those in Eq. (33), although both must vanish on the respective boundaries, that is,

$$\begin{aligned} &\delta\mathbf{v} \in U^0, \quad U^0 = \left\{ \delta\mathbf{v} \mid \delta\mathbf{v} \ \in \mathcal{C}^0 \ , \quad \delta\mathbf{v} = 0 \quad \text{on} \quad \Gamma_d \right\} \\ &\delta u_w \in V^0, \quad V^0 = \left\{ \delta u_w | \delta u_w \in \mathcal{C}^0 \ , \quad \delta u_w = 0 \quad \text{on} \quad \Gamma_w \right\} \end{aligned} \tag{34}$$

Finally, note that under the restrictions of small deformation theory, i.e. $J \approx 1$, $n^0 = n$, and $\rho_w^0 = \rho_w$, the material parameters defined in Eq. (26) become identical to those defined in Ref. [18], that is,

$$\alpha \approx 1; \quad \frac{1}{Q} \approx n\frac{\mathrm{d}S}{\mathrm{d}u_w} + \frac{Sn}{K_w}$$

3.2. *Finite element discretization*

To derive the set of discretized finite element equations, a proper approximation for both velocity and pressure fields is required. Assuming the following approximations

$$\begin{aligned} &\mathbf{v}(\mathbf{x},t) = \dot{\mathbf{u}}(\mathbf{x},t) \approx \mathbf{N}_d(\mathbf{x})\dot{\bar{\mathbf{u}}}(t) \quad \rightarrow \quad \boldsymbol{\nabla}^s\dot{\mathbf{u}}(\mathbf{x},t) \approx \mathbf{B}_d(\mathbf{x})\dot{\bar{\mathbf{u}}}(t) \\ &u_w(\mathbf{x},t) \approx \mathbf{N}_w(\mathbf{x})\bar{\mathbf{u}}_w(t) \quad \rightarrow \quad \boldsymbol{\nabla} u_w(\mathbf{x},t) \approx \mathbf{B}_w(\mathbf{x})\bar{\mathbf{u}}_w(t) \end{aligned} \tag{35}$$

the space-discretized form of Eqs (31) and (32) can be written as

$$\begin{aligned} &\int_\Omega \mathbf{B}_d^T\boldsymbol{\sigma}\, \mathrm{d}V - \mathbf{Q}\bar{\mathbf{u}}_w - \mathbf{f}^{(1)} = 0 \\ &\widetilde{\mathbf{Q}}\dot{\bar{\mathbf{u}}} + \mathbf{S}\dot{\bar{\mathbf{u}}}_w - \mathbf{H}\bar{\mathbf{u}}_w - \mathbf{f}^{(2)} = 0 \end{aligned} \tag{36}$$

DOI: 10.1002/nag

where

$$\begin{aligned}
\mathbf{Q} &= \int_{\Omega} \mathbf{B}_d^T \chi \mathbf{m} \mathbf{N}_w \, \mathrm{d}\Omega \\
\widetilde{\mathbf{Q}} &= \int_{\Omega} \mathbf{N}_w^T S \alpha \mathbf{m} \mathbf{B}_d \, \mathrm{d}\Omega \\
\mathbf{S} &= \int_{\Omega} \mathbf{N}_w^T \frac{1}{Q} \mathbf{N}_w \, \mathrm{d}\Omega \\
\mathbf{H} &= \int_{\Omega} \mathbf{B}_w^T \frac{\hat{k}}{\rho_w^0 g} \mathbf{B}_w \, \mathrm{d}\Omega \\
\mathbf{f}^{(1)} &= \int_{\Gamma_t} \mathbf{N}_d^T \widetilde{\mathbf{t}} \, \mathrm{d}S + \int_{\Omega} \mathbf{N}_d^T \hat{\rho} \mathbf{g} \, \mathrm{d}\Omega \\
\mathbf{f}^{(2)} &= \int_{\Gamma_q} \mathbf{N}_w^T \frac{\rho_w}{\rho_w^0} \widetilde{q} \, \mathrm{d}\Omega - \int_{\Omega} \mathbf{B}_w^T \frac{\hat{k}}{\rho_w^0 g} \rho_w \mathbf{g} \, \mathrm{d}\Omega
\end{aligned} \tag{37}$$

and $\mathbf{m}$ is the matrix form of the identity tensor $\mathbf{I}$. The set of equations (36) must be discretized in time as well. By using a conventional Euler backward integration scheme, the following relations are obtained

$$\begin{aligned}
\mathbf{r}_{t+\Delta t}^{(1)} &= \left(\int_{\Omega} \mathbf{B}_d^T \boldsymbol{\sigma} \, \mathrm{d}\Omega \right)_{t+\Delta t} - \mathbf{Q}_{t+\Delta t} \bar{\mathbf{u}}_w^{t+\Delta t} - \mathbf{f}_{t+\Delta t}^{(1)} \\
\mathbf{r}_{t+\Delta t}^{(2)} &= \widetilde{\mathbf{Q}}_{t+\Delta t} \bar{\mathbf{u}}^{t+\Delta t} + (\mathbf{S}_{t+\Delta t} - \Delta t \, \mathbf{H}_{t+\Delta t}) \bar{\mathbf{u}}_w^{t+\Delta t} - \Delta t \, \mathbf{f}_{t+\Delta t}^{(2)}
\end{aligned} \tag{38}$$

The above equations are nonlinear, and a general Newton–Raphson scheme is required. Using an iterative algorithm leads to

$$\begin{bmatrix} \mathbf{K}_{t+\Delta t} & -\mathbf{Q}_{t+\Delta t} \\ \widetilde{\mathbf{Q}}_{t+\Delta t} & \mathbf{S}_{t+\Delta t} - \Delta t \, \mathbf{H}_{t+\Delta t} \end{bmatrix} \begin{Bmatrix} \delta \bar{\mathbf{u}}^{t+\Delta t} \\ \delta \bar{\mathbf{u}}_w^{t+\Delta t} \end{Bmatrix}_i = - \begin{Bmatrix} \mathbf{r}_{t+\Delta t}^{(1)} \\ \mathbf{r}_{t+\Delta t}^{(2)} \end{Bmatrix}_i \tag{39}$$

where

$$\begin{aligned}
\left(\bar{\mathbf{u}}^{t+\Delta t}\right)_{i+1} &= \left(\bar{\mathbf{u}}^{t+\Delta t}\right)_i + \left(\delta \bar{\mathbf{u}}^{t+\Delta t}\right)_i \\
\left(\bar{\mathbf{u}}_w^{t+\Delta t}\right)_{i+1} &= \left(\bar{\mathbf{u}}_w^{t+\Delta t}\right)_i + \left(\delta \bar{\mathbf{u}}_w^{t+\Delta t}\right)_i
\end{aligned} \tag{40}$$

and

$$\mathbf{K} = \int_{\Omega} \mathbf{B}_d^T \mathbb{D}_T \mathbf{B}_d \, \mathrm{d}\Omega \tag{41}$$

where $\mathbb{D}_T$ is the tangential stiffness operator, which has been defined in the previous section.

DOI: 10.1002/nag

4. NUMERICAL SIMULATIONS

4.1. Deviatoric hardening model

The simulations presented here employ the framework of deviatoric hardening (cf. [21]). Within this approach, the loading surface $f = f(\boldsymbol{\sigma}, \kappa, \zeta)$ is defined as

$$f = \sqrt{3}\bar{\sigma} - \eta\, \mathrm{g}(\theta)(\sigma_m + c\cot\phi) = 0 \tag{42}$$

Here, $\sigma_m = -\boldsymbol{\sigma} : \mathbf{I}/3$, $\bar{\sigma} = \sqrt{J_2} = \sqrt{1/2\, \mathbf{s} : \mathbf{s}}$, and $\theta = \sin^{-1}\left(-3\sqrt{3}J_3/2\bar{\sigma}^3\right)/3$, where $\mathbf{s}$ is the stress deviator and $J_3 = {}^1/_3(\mathbf{s}\cdot\mathbf{s} : \mathbf{s})$. The parameter θ represents Lode's angle and is defined within the interval $-\pi/6 \le \theta \le \pi/6$, whereas $g(\theta)$ satisfies $\mathrm{g}(\pi/6) = 1$ and $\mathrm{g}(-\pi/6) = K$, where K is a constant. In Eq. (42), ϕ is the friction angle and c is the cohesion. The specific mathematical expression for $g(\theta)$ implemented here is that proposed by Willam-Warnke [22]. The hardening parameter $\eta = \eta(\kappa)$ is defined using the following hyperbolic form

$$\eta = \eta_f \frac{\kappa}{A + \kappa} \tag{43}$$

where A is a material constant and η_f defines the value of η at failure, i.e. $\eta \to \eta_f$ for $\kappa \to \infty$. Assuming that the conditions at failure are consistent with Mohr–Coulomb criterion, we have $\eta_f = 6\sin\phi/(3 - \sin\phi)$. Furthermore, the flow rule is assumed to be nonassociated, and the potential function is taken in the form

$$\psi = \sqrt{3}\bar{\sigma} + \eta_c(\sigma_m + c\cot\phi)\ln\frac{\sigma_m + c\cot\phi}{\sigma_m^0} = 0 \tag{44}$$

where $\eta_c = \text{const.}$ is a material constant.

To incorporate the deviatoric hardening model in the chemoplasticity framework, the strength parameters η_f and c, as well as the Young's modulus E, are assumed to undergo a progressive degradation in the course of chemical interaction. The evolution laws are taken in a simple linear form

$$\begin{aligned} \eta_f &= \eta_f^0(1 - G_1\zeta) \\ c &= c^0(1 - G_2\zeta) \\ E &= E^0(1 - G_3\zeta) \end{aligned} \tag{45}$$

where G's are material constants and the kinetics of the interaction process, namely evolution of ζ, is governed by Eq.(1). Note that, given the last equation in (45), the elastic operator $\mathbb{D}$ satisfies

$$\begin{aligned} \mathbb{D} &= \mathbb{D}^0(1 - G_3\zeta) \\ \mathbb{D}^{-1} &= \mathbb{D}^{0-1}/(1 - G_3\zeta) \end{aligned} \quad \to \quad \mathbb{D}^0 : \mathbb{D}^{0-1} = \mathbb{I} \tag{46}$$

so that

$$\mathbb{D} : \partial_\zeta \mathbb{D}^{-1} = h(\zeta)\mathbb{I}; \qquad h(\zeta) = \frac{G_3}{(1 - G_3\zeta)} \tag{47}$$

Hence, the fourth-order tensor $\mathbb{A}$ defined in the previous section takes the form

$$\mathbb{A} = \mathbb{I} + \Delta\zeta\left(\mathbb{D} : \partial_\zeta \mathbb{D}^{-1}\right) = (1 + \Delta\zeta h(\zeta))\mathbb{I} \quad \to \quad \mathbb{A}^{-1} = \frac{1}{1 + \Delta\zeta h(\zeta)}\mathbb{I} \tag{48}$$

DOI: 10.1002/nag

In what follows, some numerical examples are provided. The first one, which deals with the point integration algorithm, is focused on examining the effect of water injection in a sample subjected to a sustained deviatoric load of a prescribed intensity. The second example deals with an initial boundary-value problem, which involves assessment of slope stability under conditions of an intense rainfall.

4.2. *Example 1*

The first example involves a sample of a cohesive soil that is tested in triaxial compression under some initial confining pressure. The sample, in its natural state of compaction, is subjected to an axial load of a prescribed magnitude, which is subsequently kept constant while the water is said to be injected. The latter results in time-dependent degradation of mechanical properties, which stems from chemical interaction taking place in the neighborhood of interparticle contacts.

The mechanical properties of the material, in its initial state, are taken as

$$K = 100 \text{ MPa}, \quad G = 45 \text{ MPa}, \quad c = 50 \text{ kPa}, \quad \eta_f = 1.4, \quad \eta_c = 1.2, \quad A = 0.0005$$

Note that c represents here the *apparent* cohesion, which results from interparticle bonding, and it is subsequently lost upon wetting. The degradation parameters, related to chemical interaction, are assumed as

$$G_1 = 20\%, \quad G_2 = 100\%, \quad G_3 = 50\%, \quad B = 0.92$$

The constant B is chosen in such a way that at $t = 5$ s, the parameter ζ, Eq. (1), reaches the value of 0.99, that is, 99% of the reaction is said to be completed. The simulations correspond to initial confining pressure of $p = -500$ kPa. The water injection is assumed to be instantaneous, so that the problem is solved by employing the point integration scheme, as discussed earlier.

The key results are presented in Figures 1 and 2. Figure 1 shows the time-dependent history of axial strain corresponding to different deviatoric stress intensities $q = \sigma_3 - \sigma_1$, ranging from 800 to 1000 kPa. Note that for the first stage of loading, that is, application of deviatoric stress q, the response is time independent as it is governed by standard plasticity framework. Figure 2 shows the time history of η/η_f. The value of the parameter η is evaluated here from Eq. (42), so that

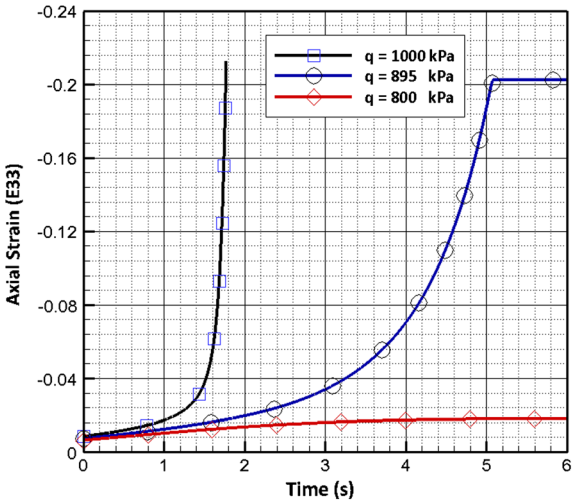

Figure 1. Displacement history versus time.

DOI: 10.1002/nag

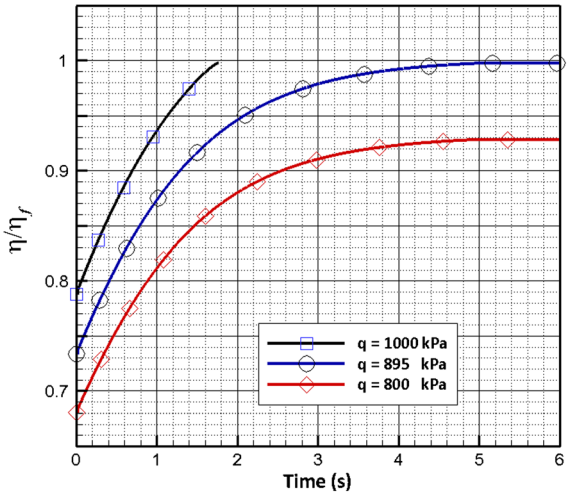

Figure 2. Value of η/η_f versus time.

$$\eta = \frac{\sqrt{3}\bar{\sigma}}{g(\theta)(\sigma_m + c\cot\phi)} \tag{49}$$

whereas at failure, there is $\eta = \eta_f$. Thus, the ratio $\eta/\eta_f \subset [0,1]$ is indicative of the extent of damage within the material.

It is evident from Figures 1 and 2 that if the wetting commences at low values of deviatoric stress intensities, that is, $\eta/\eta_f < 0.7$, the stationary conditions are reached. At higher intensities, the degradation of strength properties upon wetting triggers a spontaneous failure of the sample.

4.3. Example 2

The numerical analysis presented here involves a slope in a cohesive soil (clay) subjected to a period of an intense rainfall. The slope examined in this study has dimensions typical of engineered slopes in Singapore; it is also representative of shallow slopes in the province of Manitoba (Canada) that underwent a translational failure in the late 1990s. A major rainfall event of a prescribed intensity is considered. Note that the actual amount of rainfall that can infiltrate the ground at a given time ranges from zero to infiltration capacity, which depends on moisture content and porosity of the specific soil. Apparently, if the precipitation rate exceeds the infiltration rate, runoff will usually occur. In the simulations presented here, no antecedent rainfall is applied prior to the major event.

The numerical analysis incorporates the transient coupled formulation for unsaturated flow, as described in Section 3. As indicated earlier, the primary purpose of employing this framework lies in its ability of tracing the evolution of the phreatic surface. In the simulations, the progress of the wetting front is monitored, and the framework of chemoplasticity (Section 2.1) is used to model the evolution of mechanical characteristics of clay. The overall stability of the slope is assessed by examining the time history of the parameter η/η_f, Eq. (49), which defines the extent of damage.

The simulations were carried out assuming the following material parameters

$$E = 100\ \text{MPa}, \quad v = 0.35, \quad \eta_f = 0.98, \quad \eta_c = 0.77, \quad c = 20\ \text{kPa}, \quad A = 1.0 \times 10^{-5}$$

The kinetics of the chemical interaction and the degradation constants were selected as

$$G_1 = 10\%, \quad G_2 = 75\%, \quad G_3 = 10\%, \quad B = 460.0$$

and the parameters governing the fluid flow were taken as

DOI: 10.1002/nag

$$\mathbf{k} = 0.86\,\mathbf{I}\ (\mathrm{m/day}), \quad k_s \approx 1.0, \quad e = 1.0$$

Note that although the choice of these parameters is somewhat arbitrary, their values are typical for lightly overconsolidated clayey deposits. It needs to be emphasized that the example given here serves primarily as an illustration of the proposed methodology, so that the quantitative aspects are rather secondary.

The loading process incorporated two stages. The first one involved the solution due to the own weight of the material, and the second one was the simulation of the infiltration process and its coupling with the mechanical response. Figure 3 shows the geometry of the problem and the boundary conditions corresponding to the first stage. The total height of the slope was taken as $H = 10$ m. The gravity load was applied incrementally in five layers, to reflect the construction sequence. The key results are shown in Figures 4 and 5. Figure 4 shows the distribution of η/η_f, whereas Figure 5 gives the corresponding distribution of equivalent plastic strains at the end of construction stage. Here, the maximum value of η/η_f is 0.8, which clearly indicates that the slope is stable.

Figure 6 presents the boundary conditions for the second stage of the analysis, i.e. infiltration process. In this phase, the slope is said to be exposed to a heavy rainfall (i.e., precipitation in excess of 0.75 cm/h). Along the ground surface, the water pressure is assumed to increase linearly from an initial value of 5 kPa (suction), which corresponds to $S = 5\%$, to zero in a period of 4 h and then is maintained constant. Such boundary conditions are analogous to those in Ref. [20] and imply that the horizontal surfaces can absorb water at the rate that depends on the permeability, whereas the

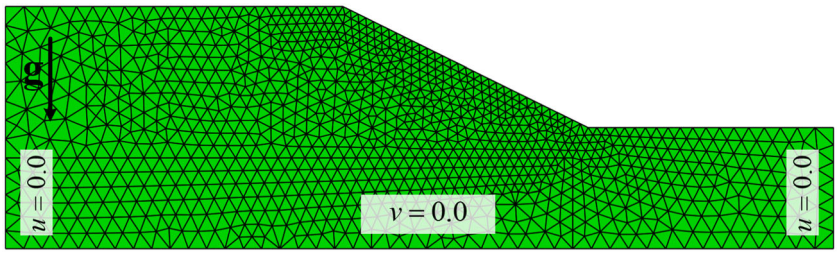

Figure 3. Geometry and boundary conditions for dry analysis under its own weight.

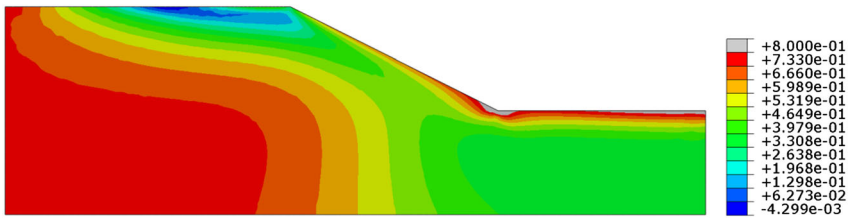

Figure 4. Value of η/η_f at the end of dry analysis.

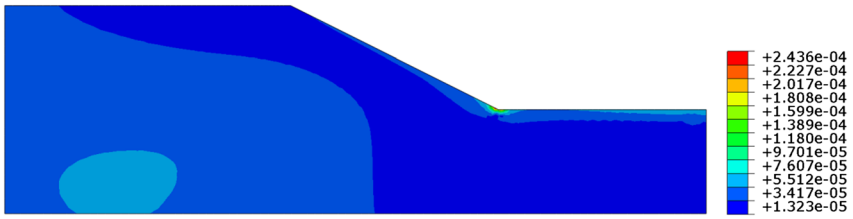

Figure 5. Equivalent plastic strain at the end of dry analysis.

DOI: 10.1002/nag

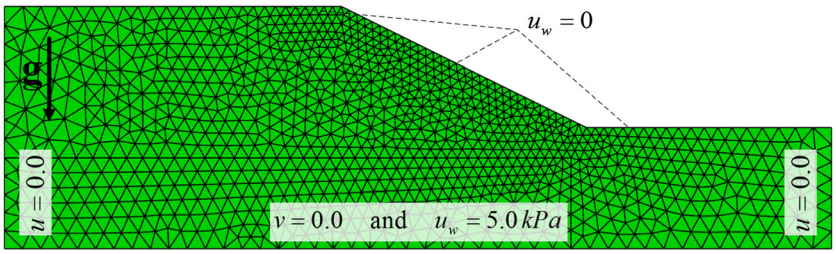

Figure 6. Geometry and boundary conditions in infiltration analysis followed by dry analysis.

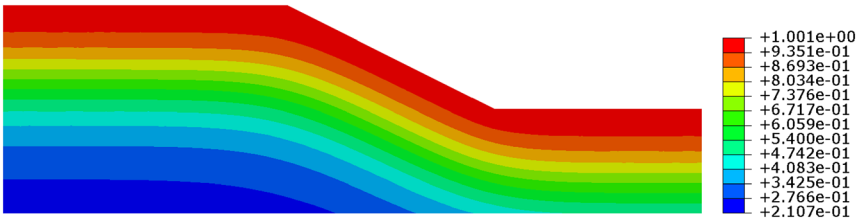

Figure 7. Saturation at the end of rainfall (30 days).

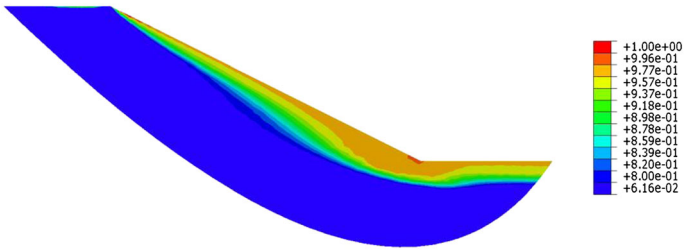

Figure 8. Value of η/η_f at the end of rainfall (30 days).

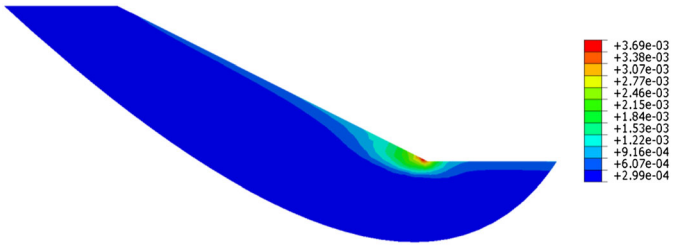

Figure 9. Equivalent plastic strain at the end of rainfall (30 days).

water cannot congregate along the slope. In addition, a suction pressure of $u_w^0 = 5$ kPa is applied at the bottom. This ensures that water can flow out of the domain, which, in turn, implies that the groundwater level (which was initially far below the ground surface) cannot be affected by this rainfall.

The infiltration analysis was performed for a period of 30 days. Figure 7 shows the distribution of the degree of saturation at the end of rainfall, whereas Figure 8 presents the corresponding contours of η/η_f. It is evident now that, in a large area around the slope, there is $\eta/\eta_f \rightarrow 1$. The latter is indicative of a failure of the slope in this region. Finally, Figure 9 shows the corresponding distribution of the equivalent plastic strain.

DOI: 10.1002/nag

5. FINAL REMARKS

In this paper, a methodology for modeling a coupled hydromechanical response of clayey soils has been presented. Within this framework, as long as the water phase is discontinuous, the material is treated as a single-phase medium undergoing evolution of mechanical properties as a result of chemomechanical interactions. At this level of saturation, the approach does not require a specification of suction–saturation relationship as the suction pressure is said to be the product of an interaction of a complex system of mineralogical and chemical factors.

A return mapping algorithm has been developed for the proposed chemoplasticity framework. In analyzing the problem of slope infiltration, the backward Euler scheme has been combined with subincrementation. This was primarily because the chemical degradation is very fast and small increments are required to obtain an accurate solution for the local stress trajectories. This algorithm significantly improves the convergence of the global solution for unsaturated flow in porous media.

The governing equations for the fluid flow in unsaturated media have been derived here using a continuum framework that incorporates the notion of a deformable control volume. The final set of equations for the discretized system is the same as that obtained using a classical approach, viz. Ref. [18].

The primary application given here involved a coupled hydromechanical analysis of a slope exposed to an intense rainfall. It was demonstrated that the water infiltration may trigger a loss of stability resulting from degradation of strength properties. The assessment of stability itself was based on examining the distribution of the ratio η/η_f that is indicative of the extent of damage. For quantitative purposes, such an assessment is rather restrictive, and a more accurate representation is required. Therefore, the future work will focus on development and implementation of numerical procedures that account for modeling of localized failure. These will involve the use of extended finite element method [23] and/or the procedures incorporating the volume averaging in the neighborhood of the shear zone [24].

REFERENCES

1. Blatz JA, Ferreira NJ, Graham J. Effects of near-surface environmental conditions on instability of an unsaturated soil slope. *Canadian Geotechnical Journal* 2004; **41**:1111–1126.
2. Griffiths DV, Mines US, Lu N. Unsaturated slope stability analysis with steady infiltration or evaporation using elasto-plastic finite elements. *International Journal for Numerical & Analytical Methods in Geomechanics* 2005; **29**:249–267.
3. Chen Q, Zhang L. Three-dimensional analysis of water infiltration into the Gouhou rockfill dam using saturated unsaturated seepage theory. *Canadian Geotechnical Journal* 2006; **43**:449–461.
4. Schmertmann JH. Estimating slope stability reduction due to rain infiltration mounding. *Journal of Geotechnical and Geoenvironmental Engineering* 2006; **132**(9):1219.
5. Tsaparas I, Rahardjo H, Toll D, Leong EC. Controlling parameters for rainfall-induced landslides. *Computers and Geotechnics* 2002; **29**(1):1–27.
6. Cho SE, Lee SR. Instability of unsaturated soil slopes due to infiltration. *Computers and Geotechnics* 2001; **28**(3):185–208.
7. Nitao J, Bear J. Potentials and their role in transport in porous media. *Water Resources Research* 1996; **32**(2):225–250.
8. Pietruszczak S. On the mechanical behaviour of concrete subjected to alkali-aggregate reaction. *Computers & Structures* 1996; **58**(6):1093–1097.
9. Hueckel T. Chemo-plasticity of clays subjected to stress and flow of a single contaminant. *International Journal for Numerical & Analytical Methods in Geomechanics* 1997; **21**(1):43–72.
10. Pietruszczak S, Lydzba D, Shao JF. Modelling of deformation response and chemo-mechanical coupling in chalk. *International Journal for Numerical & Analytical Methods in Geomechanics* 2006; **30**(10):997–1018.
11. Pietruszczak S, Pande GN. On the mechanical response of partially saturated soils at low and high degrees of saturation. In *Numerical Models in Geomechanics*, Pietruszczak S & Pande GN (*eds*.) 1995:33–39.
12. Pietruszczak S, Pande GN. Constitutive relations for partially saturated soils containing gas inclusions. *J Geotech Eng* 1996; **122**:50–59.
13. Fredlund DG, Rahardjo H. *Soil Mechanics for Unsaturated Soils*. Wiley-Interscience: New York, 1993.
14. Nuth M, Laloui L. Effective stress concept in unsaturated soils: clarification and validation of a unified framework. *International Journal for Numerical & Analytical Methods in Geomechanics* 2008; **32**:771–801.
15. Alonso E, Gens A, Josa A. A constitutive model for partially saturated soils. *Géotechnique* 1990; **40**:405–430.
16. Crisfield MA. *Non-linear Finite Element Analysis of Solids and Structures*. Advanced topics, Vol. **2**. Wiley: New York, 1997.
17. Simo J. *Computational Inelasticity*. Springer Verlag: New York, 1998.

DOI: 10.1002/nag

18. Zienkiewicz O, Chan A, Pastor M, Schrefler B. *Computational Geomechanics*. Wiley: New York, 1999.
19. Sanavia L. Numerical modelling of a slope stability test by means of porous media mechanics. *Engineering Computations* 2009; **26**(3):245–266.
20. Borja RI, White JA. Continuum deformation and stability analyses of a steep hillside slope under rainfall infiltration. *Acta Geotechnica* 2010; **5**(1):1–14.
21. Pietruszczak S. *Fundamentals of Plasticity in Geomechanics*. CRC Press, 2010.
22. Willam K, Warnke E. Constitutive model for the triaxial behaviour of concrete, *IABSE Seminar on Concrete Structures Subjected to Triaxial Stresses* III-1, 184, 1974 n.d.
23. Belytschko T, Black T. Elastic crack growth in finite elements with minimal remeshing. *International Journal for Numerical Methods in Engineering* 1999; **45**(5):601–620.
24. Pietruszczak S. On homogeneous and localized deformation in water-infiltrated soils. *International Journal of Damage Mechanics* 1999; **8**(3):233–253.

DOI: 10.1002/nag